HHS Public Access

Author manuscript

*J Phys Chem B*. Author manuscript; available in PMC 2016 February 16.

Published in final edited form as:

*J Phys Chem B*. 2008 March 20; 112(11): 3509–3521. doi:10.1021/jp709729d.

# Understanding the Dielectric Properties of Liquid Amides from a Polarizable Force Field

**Edward Harder**[†], **Victor M. Anisimov**[‡], **Troy Whitfield**[§], **Alexander D. MacKerell Jr.**[*,‡], and **Benoît Roux**[*,†]

Department of Biochemistry and Molecular Biology, Center for Integrative Science, University of Chicago, Chicago, Illinois 60637, Department of Pharmaceutical Sciences, School of Pharmacy, University of Maryland, Baltimore, Maryland 21201, and Bioscience Division, Mathematics and Computer Science Division, Argonne National Laboratory, Argonne, Illinois 60439

## Abstract

The role played by electronic polarization in the dielectric properties of liquid *N*-methyl acetamide (NMA) is examined using molecular dynamics simulations with a polarizable force field based on classical Drude oscillators. The model presented is the first force field shown to reproduce the anomalously large dielectric constant of liquid NMA. Details of the molecular polarizability are found to be important. For instance, all elements of the polarizability tensor, rather then just the trace, impact on the condensed phase properties. Two factors related to electronic polarizability are found to contribute to this large dielectric constant. First is the significant enhancement of the mean amide molecular dipole magnitude, which is 50% larger in the liquid than in the gas phase. Second is the consequent strong hydrogen bonding between molecular neighbors that enhances the orientational alignment of the molecular dipoles. Polarizable models of amide compounds that have two (acetamide) and zero (*N*,*N*-dimethyl acetamide) polar hydrogen-bond donor atoms are also investigated. Experimentally, the neat liquid dielectric constants at 373 K are 100 for NMA, 66 for acetamide and 26 for *N*,*N*-dimethyl acetamide. The polarizable models replicate this trend, predicting a dielectric constant of 92 ± 5 for NMA, 66 ± 3 for acetamide and 23 ± 1 for *N*,*N*-dimethyl acetamide.

## 1. Introduction

Understanding the physical nature of interactions underlying the energy landscape of proteins is a crucial step toward establishing a thorough understanding of their structure, dynamics, and function. The class of models commonly referred to as molecular mechanics force fields[1–4] aims to address this issue by parsing the interaction energy into atomic-level contributions that approximate the salient physical features necessary in the study of biomolecular systems. Harmonic oscillators replace intramolecular vibrations, the Lennard-

[*] Corresponding authors. (B.R.) roux@uchicago.edu; (A.D.M.) alex@outerbanks.umaryland.edu..
[†]University of Chicago.
[‡]University of Maryland.
[§]Argonne National Laboratory.

**Supporting Information Available:** The model parameters. This material is available free of charge via the Internet at http://pubs.acs.org.

Jones (LJ) function replaces electronic repulsion, and dispersion and fixed-point charges approximate the electrostatic interactions.

Such force fields depend on parameters that are empirically adjusted to reproduce, as much as possible, a body of experimental data. The chemical environment of proteins is complex, which makes teasing out energetic contributions from particular chemical motifs and attributing these to specific terms in the force field a challenge. A reasonable strategy to determining such parameters is to focus on small organic molecule analogs to the functional groups that constitute the biomolecule. Interactions in the gas phase can be probed by high-level quantum mechanical (QM) calculations, which are computationally tractable for small molecules. Interactions in condensed phase environments can be inferred from thermodynamic, transport, and dielectric properties that are readily available for many organic materials.

At the core of protein structures is the polypeptide backbone, which is made up of amide-like units that carry a dipole extending from the carbonyl oxygen to the polar amide hydrogen. Hydrogen bonding between the amide hydrogen of one peptide and the carbonyl oxygen of another plays a critical role in the stabilization of secondary structural elements such as beta sheets and alpha helices.[5–9] Properly modeling the electrostatics of these amide units and capturing accurately the nature of amide backbone hydrogen bonding is thus a key element in constructing an accurate protein force field.

In this report, we study *N*-methyl acetamide (NMA) as the small molecule analog of the peptide linkage. The importance of the amide functional group in biology has led to an extensive list of literature on the study of the properties of small amide molecules, including the dielectric properties of their neat liquids.[10–15] Of note is the anomalously large dielectric constant for the N-methylated amides.[11,12] This property, which is a measure of the macroscopic zero frequency response to an external electric field, is expected to depend on the magnitude of the individual molecular dipoles and their spatial correlation.[16] Past efforts to explain this phenomenon have noted that strong local association through amide hydrogen-bonding could lead to cooperatively aligned molecules in liquid NMA and, thus, considerable dipolar correlation.[11,12]

The sensitivity of the dielectric constant to amide hydrogen-bonding suggests that it should be an important benchmark in the calibration of the model. Even so, this property has been characterized for only a few biomolecular force field models. This is in part due to the extensive sampling necessary to accurately determine the dielectric constant.[17] Recent work on the CHARMM force field has found that the model underestimates the dielectric constant of liquid NMA by nearly 70%.[17] The dielectric constant of liquid formamide calculated using the OPLS/AA force field found it to underestimate the experimental value by nearly 50%.[18] The failure to reproduce the dielectric properties of these amide liquids appears to be in part a consequence of the mean field approximated fixed charges used in these force fields to account for electronic polarization. The electrostatics of these fixed-charge models takes a mean field account of electronic polarization. Atomic charges are adjusted to approximate the average electrostatic response in a condensed phase environment, but are not allowed to change in response to varying electric fields. It may be that fixed charge

models parametrized for environments that can be alternately polar and nonpolar, such as that found in proteins, may not adequately capture the electrostatics in a homogeneously polar environment such as liquid NMA. The difficulties in determining a unique optimal mean field approximation and the discrepancy between these models and experiment reach beyond the mere technicalities of force field parametrization. The failure clearly signals that some fundamental aspect of the electrostatic properties of liquid NMA is systematically misrepresented when induced polarizability is not explicitly included.

As part of an ongoing effort to build a polarizable force field for biomolecules using classical Drude oscillators,[19–27] we present a polarizable model for NMA that accurately captures the dielectric properties of the neat liquid. The addition of electrostatic polarization to a model is not without complication. In Sections 3.1 and 3.2, two issues that sensitively impact the dielectric properties of the polarizable model are addressed: (1) ad hoc reduction of the model's molecular polarizability relative to the computed QM gas-phase value. This reduction is typically done to effectively account for Pauli exclusion effects that occur in the condensed phase.[19,28] (2) The sensitivity of the liquid dielectric properties to the orientation of the Drude model molecular polarizability tensor. In Section 3.2, the dielectric properties of the Drude NMA model are compared with that of a nonpolarizable model to elucidate the role played by electronic polarization. In Section 3.3, the gas-phase energetic properties of the model are summarized along with thermodynamic, dielectric, and dynamic condensed phase properties. Finally, in Section 3.4, results are presented for the dielectric properties over a series of amide models, including an analog of amide-like amino side chains (acetamide) and a fully methylated amide (*N*,*N*-dimethyl acetamide).

## 2. Methods

### 2.1. Model

To model the electronic polarization of a given atom, a mobile auxiliary particle carrying a charge, $q^{\mathrm{D}}$, is introduced and attached to the atom by a harmonic spring. A charge of opposite sign is added to the atom, and the electro-neutral pair forms a classical Drude oscillator, which polarizes in response to an external field. The model consists of “core” charges, $q_i$, associated with either atomic or virtual lone pair sites; as well as the Drude charges, $q_i^{\mathrm{D}}$ and $-q_i^{\mathrm{D}}$, associated with the electroneutral oscillators. Drude oscillators are added to heavy atoms with the positive end ($q_i^{\mathrm{D}}$) anchored to the atomic site. The total charge on atom sites with a core and Drude charge is thus $q_i+q_i^{\mathrm{D}}$. The model potential energy is

$$U=U_{\mathrm{internal}}+U_{LJ}+U_{\mathrm{self}}+U_{\mathrm{elec}} \quad (1)$$

where $U_{\mathrm{internal}}$ includes energy terms for bonds, angles, and dihedrals; $U_{\mathrm{LJ}}$ is the Lennard-Jones potential energy; and $U_{\mathrm{self}} + U_{\mathrm{elec}}$ represents the electrostatic potential energy. The associated functional forms for $U_{\mathrm{internal}}$ and $U_{\mathrm{LJ}}$ have been discussed elsewhere.[1]

$U_{self}$ is the harmonic self-energy of the Drude oscillators. For most of the atoms, the self-energy is expressed as a single spherically isotropic spring, $U_{self} = (1/2)K^{(D)}d^2$. More generally, for an anisotropic oscillator, it can be written as

$$\begin{aligned} U_{self} &= \mathbf{d} \bullet \mathbf{K}^{(D)} \bullet \mathbf{d} \\ &= \left[\mathbf{K}_{11}^{(D)}\right] d_1{}^2 + \left[\mathbf{K}_{22}^{(D)}\right] d_2{}^2 + \left[\mathbf{K}_{33}^{(D)}\right] d_3{}^2 \end{aligned} \quad (2)$$

where $d_1$, $d_2$, and $d_3$ are the projection of the Drude displacement vector **d** on orthogonal axes defined using a local intramolecular reference frame. For example $d_1 = \mathbf{d}\cdot\hat{n_{A,B}}$ where $\hat{n_{A,B}}$ is a unit vector directed between atoms A and B in the molecule of interest. In accord with the Born–Oppenheimer approximation, the electrostatic degrees of freedom in the model are relaxed to their energy minimum for any given nuclear configuration. The result is an equilibrium between the force of the Drude spring and the electrostatic force from the total external electric field, $\mathbf{K}_i^D\mathbf{d}_i = -q_i^D\mathbf{E}_i$, where $\mathbf{E}_i$ is the total electric field at the position of the Drude particle, $\mathbf{r}^D$. This condition can be written in a form analogous to the self-consistent field (SCF) equation for atomic point dipoles, $\mu_i = \alpha_i^D\mathbf{E}_i$. The isotropic polarizability ($\alpha_{iso,\,i}^D = Tr\left(\alpha^D\right)/3$) and force constant ($K_{iso}$ = 500 kcal/mol/Å$^2$) are used to define the charge of the Drude oscillator,

$$q_i^D = \sqrt{\alpha_{iso}^D / K_{iso}} \quad (3)$$

The atomic polarizability tensor associated with each Drude oscillator is then related to the components of the force constant tensor by

$$\alpha^D = -\left(q_i^D\right)^2\left(\mathbf{K}_i^D\right)^{-1} \quad (4)$$

The term $U_{elec}$ corresponds to the sum over all Coulombic interactions between the core charges $q_i$, located at $\mathbf{r}_i$, and the Drude charges $-q_i^D$ and $q_i^D$, located at $\mathbf{r}_i$, and $\mathbf{r}_i^D = \mathbf{r}_i + \mathbf{d}_i$, respectively. The interactions of the various pairs of charges are treated according to the topological bonding order determined from the atoms in the molecule. As in standard fixed-charge force fields, the interactions between core charges corresponding to 1–2 (neighbor) and 1–3 (next-neighbor) pairs are subsumed by explicit bonding terms in the potential energy, $U_{internal}$, and necessarily excluded from the electrostatic energy. Similarly, the interactions of the Drude oscillators with core charges are excluded for 1–2 and 1–3 pairs. The Coulomb interactions between Drude oscillators corresponding to 1–2 and 1–3 atom pairs are present and screened by the function $S_{ij}$.[29] The general form of the screening function used in this work is

$$S_{ij}\left(r_{ij}\right) = 1 - \left(1 + \frac{\left(a_i + a_j\right) r_{ij}}{2\left(\alpha_i\alpha_j\right)^{1/6}}\right) e^{-\left(a_i + a_j\right) r_{ij} / \left(\alpha_i\alpha_j\right)^{1/6}} \quad (5)$$

where $r_{ij}$ is the distance between Drude charges, $\alpha_i$ is the trace of the atomic polarizability tensor, and the Thole damping parameters, $a_i$, modulate the screening strength of $S_{ij}$. The

interactions involving all core charges and all Drude oscillators are included for all 1–4 pairs and beyond without screening.

### 2.2. Parametrization Protocol

A procedure for determining core and Drude charges,[22,21] similar in spirit to work by Friesner and co-workers,[28,30–33] is generalized to include Thole damping parameters (see eq 5) and applied to the amide models in this work. Briefly, a map of the electrostatic potential (ESP) that surrounds the model compound monomer is evaluated on a set of specified grid points using density functional theory computations at the B3LYP/aug-cc-pVDZ[34,35] level. To measure the electronic response of the molecule, a series of perturbed ESP maps is computed by placing a single +0.5*e* test charge at chemically relevant positions around the molecule. The same calculations are repeated using our Drude model, restricting the force constant tensor of each oscillator to be isotropic. Optimal parameters are chosen to minimize the difference between the QM and Drude ESP maps with additional parametrical restraints.[21,22] Most of the Drude oscillators in the current force field are isotropic. An exception is made for atomic sites bearing lone pairs. In this study, only the Drude oscillator on the oxygen atom of the amide group is made anisotropic. The presence of lone pairs on carbonyl oxygen has been shown to give rise to a local electrostatic potential that is not precisely captured by an atom centered charge and isotropic Drude oscillator.[22] To account for this in the force field, the core oxygen charge is restrained to virtual site positions, and the Drude oscillator on carbonyl oxygen is made anisotropic. The virtual site geometry and the components of the oscillator force constant tensor are not part of the fitting procedure used to minimize the difference in ESP maps discussed above. The virtual site geometry is determined by comparing to the local QM ESP in the vicinity of the oxygen atom. The force constant tensor of the oxygen Drude oscillator is determined by comparing to the local QM polarization response in the vicinity of the oxygen atom. Details of the protocol are discussed in Harder et al.[22] The search for an optimal set of LJ parameters is discussed in Section 3.1.

Equilibrium internal bond parameters were optimized against crystal data from a survey[1] of the Cambridge Crystal Data Bank.[36] Force constants were optimized against vibrational spectra and potential energy surfaces for rotation about selected dihedrals. Target condensed phase vibrational spectra of NMA were those reported in MacKerell et al.[1] and Herrebout.[37] The energy associated with the O–C–N–C torsion is optimized against an experimental estimate[38] for the barrier height of 20 kcal/mol and a predicted cis/trans energy of 2.5 kcal/mol from a QM calculation in accord with the protocol detailed in MacKerell et al.[1] A summary of the vibrational frequency and dihedral data for the final Drude model is presented in the Supporting Information.

The above procedure is used to determine an optimal parameter set for NMA. Electrostatic parameters for all three amide molecules studied are optimized using the ESP fitting protocol.[21,22] No restriction is made to keep the amide hydrogen atom charges of acetamide or the charges/polarizabilities of the nitrogen-substituted methyl groups of *N*,*N*-dimethyl acetamide equivalent during the ESP fit. The resultant asymmetry in these parameters is reflective of the asymmetry in the molecule. Upon rotation of the amide torsion, the charges/

polarizabilities will be suboptimal for the resultant conformation. Since sampling of such suboptimal fitted conformations is exceedingly rare during the course of a typical molecular dynamics simulations (a consequence of the ≈20 kcal/mol rotation barrier), we have chosen to preserve the asymmetry in these parameters rather than impose an equivalence criteria.

LJ and bond parameters that do not involve nitrogen are transferred directly from NMA to the acetamide and *N*,*N*-dimethyl acetamide models. The remaining acetamide and *N*,*N*-dimethyl acetamide parameters are optimized using the above procedure. Final parameters for all models and target data used in the parametrization is provided in the Supporting Information.

### 2.3. Computational Details

Most QM calculations were carried out using the Gaussian 03 suite of programs.[39] Vibrational spectra were computed at the MP2/6-31G(d) level with a scale factor of 0.9434[40] to supplement available experimental data in the parametrization of intramolecular bond force constants. Analysis of the vibrational spectra was performed with the MOLVIB module[41] in CHARMM using the internal coordinate assignment suggested by Pulay.[42]

Density functional theory provides an efficient means of evaluating the ESP maps used to fit electrostatic parameters of the models.[21,33] The QM ESP calculations were evaluated using the B3LYP functional[34,35] and the aug-cc-pVDZ basis set, a combination that has been shown to give good agreement with molecular polarizabilities and gas-phase dipole moments.[21] The electrostatic parameter fitting of the force field was carried out using a modified version of the FITCHARGE module in CHARMM.[43,44]

Optimized interaction energies and geometries for the model compounds with individual water molecules were obtained by scanning the energy along selected intermolecular distance coordinates while keeping the geometries of the model compound and water fixed. Geometries are optimized using MP2 with the 6-31G(d) basis set, which provides sufficient accuracy to determine hydrogen bond distances.[27,33] Interaction energies were evaluated as the difference between the resultant minimum energy conformer and the respective monomers. QM energies were calculated using MP2 with the 6-311+G(3df,2p) basis set and the removal of basis set superposition error.[45] Polarization and diffuse functions were included in the energy calculation to give a faithful representation of the polarization response. The same protocol was also used to evaluate the energy for the NMA homodimer. A similar protocol was used to evaluate the interaction energy between an NMA monomer and small clusters of NMA molecules. The large computational demands necessary to compute energies for the larger clusters motivated the use of an auxiliary basis set MP2 method for these calculations. Energies for the NMA clusters were computed using the QCHEM program[46] using RI-MP2[47,48] with the 6-311+G(3df,-2p) basis set, including a basis set superposition correction. Tests on the NMA homodimer and the interaction of an NMA molecule with a chain of two NMA molecules gave energies that agreed to within 0.5% of analogous MP2 calculations.

All molecular dynamics (MD) simulations were performed with the program CHARMM[43,44] using a velocity Verlet algorithm.[49] Simulations used to evaluate the

diffusion coefficient were run at constant temperature and a constant volume that corresponds to the experimental liquid density at the simulated temperature. All other liquid simulations were run at constant temperature and pressure. Intramolecular contributions to the hydration free energy and enthalpy of vaporization were evaluated from gas-phase simulations run at constant temperature and constant volume. The temperature and pressure in the liquid simulations were controlled by a Nosé-Hoover thermostat and Andersen-Hoover barostat, respectively.[50,51] Temperature in the monomer simulations were controlled by a Langevin thermostat.[49] All liquid simulations were performed at 1 atm. The SHAKE/Roll and RATTLE/Roll procedures[52,53] were used to constrain covalent bonds to hydrogens.

The electrostatic degrees of freedom are minimized at the outset of the simulation and propagated dynamically along with the nuclei. For appropriately chosen kinetic variables, so-called extended Lagrangian simulations provide an accurate and efficient alternative to a self-consistent field solution at each time step of the simulation.[54,55] A mass of 0.1 amu is added to the free end of the Drude oscillator and subtracted from the reference heavy atom. The equations of motion are integrated with a 1 fs time step. Although the oscillator dynamics has been shown to be approximately adiabatic with this choice of mass,[20] an additional Nosé thermostat at a temperature of 1 K is coupled to them.

Periodic boundary conditions were used in all liquid simulations. A particle mesh approximation to the Ewald sum with “tin foil” boundary conditions is used to evaluate the Coulombic interactions in the liquid simulations.[56] A smooth real space cutoff is applied between 10 and 12 Å, a Ewald splitting parameter of 0.34 $Å^{-1}$, a grid spacing of ≈1.0 Å, and a sixth-order interpolation of the charge to the grid is used. The same cutoff scheme is used for the Lennard-Jones potential, and a long range correction to the energy and pressure from the LJ potential is included.[49]

Short, neat, liquid simulations were performed on a system of 64 molecules to select satisfactory models based on the liquid density. The NMA and acetamide simulations were performed at 373 K. The *N*,*N*-dimethyl acetamide simulation was run at 298 K. Averages were taken over the last 75 ps of a 100 ps simulation. For dielectric properties of the Drude NMA models at 373 K, data from the last 1.5 ns of 40 independent 2 ns simulations were averaged. Data from the last 500 ps of 40 independent 800 ps simulations were averaged to get the dielectric data for acetamide. Data from the last 100 ps from 20 independent 200 ps simulations were averaged to get the dielectric constant of *N*,*N*-dimethyl acetamide. To evaluate the dielectric properties of Drude NMA at 308 K, 40 3-ns simulations were run, and the last 2.5 ns of each was averaged. Data from the last 600 ps of 40 1.2-ns simulations were averaged to calculate the dielectric data for the CHARMM model of NMA. The final model enthalpy of vaporization and liquid density of NMA ($T$ = 373 K) was taken from the last 300 ps of the 40 simulations used to compute the dielectric properties. Ten independent 550 ps simulations on a system of 64 molecules at 373 K were run to evaluate the diffusion constant. The final 500 ps of each was used for data collection.

The hydration free energies were computed from a box containing 118, 119 and 118 water molecules for acetamide, NMA, and *N*,*N*-dimethyl acetamide, respectively. The dispersive and repulsive contributions to the free energy were split using Weeks–Chandler Andersen

decomposition of the LJ energy.[57] The electrostatic and dispersive contributions were evaluated by thermodynamic integration. The integration was partitioned into 10 windows and performed using the trapezoid rule. The repulsive part of the free energy was evaluated from free energy perturbation using a protocol discussed elsewhere.[27,58] Averages in the free energy calculations were taken from the last 100 ps of a 200 ps simulation for each window. A long-range correction to the free energy is included. Error bars for the free energy were estimated from a block average of four 25 ps simulations.[49]

CPMD simulations were carried out for neat liquids of acetamide and *N*,*N*-dimethyl acetamide using the PINY_MD program.[59,60] These simulations used the gradient-corrected BLYP approximate density functional[34,35] and a plane-wave basis set. Calculations were performed at the Γ-point with a 70 Ry energy cutoff and norm-conserving pseudopotentials.[61] A baseline fictitious electronic mass of 475 a.u. was used with mass preconditioning.[62] The canonical ensemble was sampled using Nosé-Hoover chain thermostats[50,63–66] and a 0.125 fs time step. In order to ensure adiabaticity, the hydrogen masses were substituted with oxygen masses. CPMD simulations were carried out at 373 K on a system of 20 acetamide molecules and a system consisting of 16 *N*,*N*-dimethyl acetamide molecules, respectively. Both simulations used initial coordinates taken from well-equilibrated Drude model simulations performed in the isothermal–isobaric ensemble. The CPMD simulation of acetamide was further equilibrated for 7 ps, and data were collected during a subsequent 10 ps of simulation. For *N*,*N*-dimethyl acetamide, the CPMD simulation was equilibrated for 2 ps, followed by 5 ps of production. Molecular dipoles from the CPMD simulations were assigned through the use of maximally localized Wannier function centers.[67–69] In the case of acetamide, the Wannier function centers were computed for configurations extracted every 500 fs and every 250 fs in the case of *N*,*N*-dimethyl acetamide.

## 3. Results and Discussion

The sensitivity of the liquid dielectric constant to four types of Drude oscillator based polarizable models was investigated. The models are distinguished by the relative magnitude and anisotropy in their molecular polarizability. Furthermore, to probe the sensitivity of the dielectric constant to the LJ potential, a set of models was generated representing points on a discrete grid in the LJ parameter space for each class of polarizable model. The dielectric properties of representative LJ models in each class were then selected for further study on the basis of their agreement with QM interaction data in the gas phase and experimental determinants of the neat liquid density and hydration free energy.

### 3.1. Models

The polarizable models in this study are characterized by a molecular polarizability that depends on the atomic polarizabilities of the constituent Drude oscillators (see eq 4) and the intramolecular oscillator interactions. This model polarizability is meant to represent the electronic response of the real molecule. As discussed in Section 2.2, the parameters associated with the molecular polarizability of the model are generated from fitting to the electronic response of a QM model in the gas phase. A potential complication in selecting electro-static polarizability parameters from gas-phase data has been raised recently by work

studying the properties of liquid water. Several models with polarizability parameters reflective of the gas-phase electronic response appeared to overestimate the liquid structure and give dielectric constants that were too large as compared to experiment, leading to the suggestion that models based on the gas-phase polarizability overestimate the electro-static response in the condensed phase.[19,28] Physical arguments suggesting that Pauli repulsion between neighboring molecules can suppress the molecular electronic response in condensed phases support this notion.[26] Furthermore, analysis of the dispersion properties of alkali halide crystals[70–73] has found the atomic polarizability of atoms can be strongly affected by their environment. In a previous study of a Drude-based polarizable model of water, a polarizability 30% reduced from the gas-phase gave the best agreement with the experimental dielectric constant.[19] However, it is worth pointing out that at least one model of water seems to yield excellent results without scaling the polarizability.[74] This suggests that the issue remains in question. To analyze the impact of the magnitude of the molecular polarizability on the dielectric constant of liquid NMA, two models are examined. The first type has a molecular polarizability that corresponds to the gas phase (unscaled); the second type has its polarizability reduced by 30% (scaled), consistent with that of the aforementioned Drude polarizable water model.

In addition to the magnitude, the orientation of the molecular polarizability may also sensitively impact model properties.[75] Most of the individual atomic polarizable sites (i.e., Drude oscillators) in the current force field respond isotropically in the presence of an external electric field. An exception is made for atomic sites bearing lone pairs. For the amide molecules included in this study, only the Drude oscillator on oxygen is made anisotropic. The anisotropy of the oxygen oscillator captures local electrostatic features around the oxygen atom and is not strongly coupled to the anisotropy in the molecular polarizability. The orientation of the molecular polarizability tensor is predominantly determined by coupling between the Drude oscillators on neighboring atomic sites. In the present models, oscillators on neighboring atomic sites interact according to a screened Coulomb potential (see eq 5). Screening of the Coulomb potential is necessary to describe electrostatic interactions between point dipole-like sites at such short distances.[29] A Thole screening function in which the screening strength is modulated by a Thole parameter $a$[29] is chosen. In eq 5, $a$ corresponds to the sum $a_i + a_j$. In the limit that $a \rightarrow 0$ these interactions go to zero and the polarizability becomes isotropic, whereas in the limit that $a \rightarrow \infty$ the bare Coulomb potential is recovered. In the original work of Thole,[29] $a$ is assumed to be a constant irrespective of the atomic pair involved. The same assumption with a corresponding value of $a$ ) 2.6 has been used recently to build polarizable Drude models of alkanes, alcohols, and aromatic rings with some success.[23,24,27] Recent work on an atomic multipole-based polarizable force has also made use of this constant Thole assumption.[76] Such an empirical rule may, however, prove problematic for chemical groups such as amides, in which quantum mechanical effects such as resonance may strengthen the electronic response along a particular molecular axis relative to another. To examine the sensitivity of the model dielectric constant to the orientation of the molecular polarizability, we investigate two types of models with different short-range dipole–dipole coupling. The first (cthole) assumes a constant Thole parameter of $a = 2.6$, and the second makes $a_i$ independent variables (vthole)

that are fitted along with the Drude oscillator charges to reproduce gas-phase QM electrostatic data.

In all, four electrostatic models are examined: an unscaled polarizable model with variable Thole parameters (unscaled/vthole), a scaled polarizable model with a variable Thole parameter (screened/vthole), an unscaled polarizable constant Thole model (unscaled/cthole), and a scaled polarizable constant Thole model (scaled/cthole). The gas-phase molecular dipole and molecular polarizability tensor for these four electrostatic models compared to a QM calculation is summarized in Tables 1 and 2. The Cartesian axes are defined relative to the molecular orientation illustrated in Figure 1. In this orientation, the Cartesian axes align with the principal axes of the molecular polarizability for the Drude cthole models. The arrow is directed along the QM calculated dipole. In accord with our model definitions, the magnitude (defined as the trace of the tensor) of the molecular polarizability is in close agreement with the QM calculation for our unscaled models, and the scaled models have an approximately 30% reduced magnitude. Of note is the exaggerated anisotropy in the molecular polarizability for models that assume a constant Thole parameter (cthole). It appears that the use of a unique damping parameter to screen these oscillator interactions leads to an overestimate of the polarizability along the long axis ($x$ direction) for such amides. When the atom-type-dependent Thole parameters are used ($a_i$ in the vthole models), then excellent agreement with the QM calculation is recovered for both the magnitude and orientation of the components of the polarizability tensor.

We note that this electrostatic fitting procedure does give rise to an asymmetry in the lone pair charges around the oxygen atom of the amide molecules (see parameters given in the Supporting Information). This feature does not appear to be native to the electron charge distribution around the oxygen atom, as evidenced by the maximally localized Wannier functions[67–69] computed from these molecules using the same theory level and basis sets employed in the CPMD simulations. It is conceivable that such parametrized charges are influenced in part by portions of the electron density that surrounds the carbonyl-bound methyl group and amide nitrogen atom, respectively. One should keep in mind that the ultimate target of such electrostatic parametrization efforts is a set of charges that gives rise to an accurate electrostatic potential that is inherent to the above fitting procedure against the QM electrostatic potential data.

To investigate and find an optimal set of LJ parameters for each of these four electrostatic models, a grid of potential models is constructed on the basis of variations in the LJ parameters (see the Supporting Information for the grid details). As a simplifying assumption, we use standard aliphatic Lennard-Jones parameters for the methyl groups[23] to reduce the parameter space search. First, we are interested in determining the LJ parameters that should accurately reproduce some basic nondielectric properties of the molecule. We select a probe of gas-phase energetics (interactions with water) and probes of liquid thermodynamic properties (the neat liquid molar volume and hydration free energy) as target properties that are subsequently used to select out viable models from the grid.

Heterodimers of NMA with water are used to probe the intermolecular interactions in the gas phase. In all the Drude and QM dimer computations, the molecular geometry of NMA is

fixed at the monomer-optimized MP2/6-31G(d) level, and the water geometry is fixed to correspond to the Drude model of water.[20] For selected hydrogen-bonding configurations (see Figure 2), the energy is minimized along the illustrated intermolecular distance coordinate. Models that agree with the QM data to within 0.5 kcal/mol and within 0.15 Å of this minimized energy and geometry for each dimer configuration are selected to run (short) neat, liquid simulations. The results of the short, neat, liquid NMA simulations are presented in Figure 3. The enthalpy of vaporization is plotted as a function of the molar volume at a temperature of 373 K. Each LJ model is color-coded on the basis of their electrostatic model type (i.e., unscaled/vthole etc.). Models that lie within 0.5 $Å^3$ of the experimental molar volume are selected to run hydration free energy calculations. The experimental enthalpy of vaporization at 373 K is estimated from vapor pressure data ranging between 360 and 380 K. Estimates for the enthalpy of vaporization vary considerably (−15.1 and −13.8 kcal/mol),[77,78] and therefore, only the molar volume is used to select viable LJ models from this calculation. Figure 4 plots the results from the hydration free energy calculations against the enthalpy of vaporization. Representative LJ models that gave the best agreement with the experimental hydration free energy were chosen from each class of electrostatic model to run long, neat liquid NMA simulations to evaluate the model dielectric constant. Because the sensitivity of the dielectric properties of the Drude models is found to be greater for models with a larger molecular polarizability, a larger set of LJ models is selected from the unscaled polarizable Drude models than from the scaled polarizable models to evaluate their dielectric constant.

### 3.2. Dielectric Properties of Liquid NMA

The dielectric constant ($\varepsilon$) is the proportionality constant between the polarization ($P$) of a dielectric medium and the macroscopic electric field ($\mathbf{E}$),[79]

$$P(r) = \frac{\epsilon - 1}{4\pi}\mathbf{E}(r) \quad (6)$$

An expression for $\varepsilon$ in terms of the microscopic properties of the medium proves useful for extracting this property from a molecular dynamics simulation. For boundary conditions consistent with our simulations, $\varepsilon$ is[80]

$$\epsilon = \epsilon_\infty + \frac{4\pi}{3\langle V\rangle kT}\left(\left\langle M^2\right\rangle - \langle M\rangle^2\right) \quad (7)$$

where the system system dipole, $M = \sum_i^N \mu_i$, corresponds to a unit cell containing $N$ molecular dipoles at an average volume, $\langle V\rangle$, and temperature, T. The infinite frequency dielectric response, $\varepsilon_\infty$, is calculated from the Clausius–Mosotti approximation.[81] A more rigorous method to compute $\varepsilon_\infty$ could be used;[23] however, in a highly associative polar liquid, the dielectric constant is dominated by the fluctuations of the system dipole, and the Clausius–Mosotti approximation is sufficient. For an isotropic system, the system dipole averages to zero, and the fluctuations are

$$\left\langle M^2 \right\rangle = \sum_i^N \langle \mu_i \bullet M \rangle \quad (8)$$

For a system consisting of identical molecular dipole moment magnitudes, $|\mu|$, the purely orientational component can be factored, leaving[82]

$$\left\langle M^2 \right\rangle = N G_K |\mu|^2 \quad (9)$$

where $G_K = \left\langle \hat{\mu}_i \bullet \sum_j \hat{\mu}_j \right\rangle$ is the Kirkwood $G_K$ factor and $\hat{\mu}_i = \mu_i / |\mu_i|$.[16] According to this definition, the $G_K$ factor is a measure of the orientational correlation between molecular dipoles. Configurations that have parallel dipole alignment lead to contributions to $G_K$ that are greater than 1, and for uncorrelated dipoles, $G_K = 1$. One may also note that with the above definition, the magnitude of the molecular dipole moments for a system of polarizable molecules will be characterized by a distribution that is nontrivially coupled to their spatial correlation. In the narrow dipole distribution limit, eq 8 can be approximated by[83]

$$\left\langle M^2 \right\rangle \approx N G_K \langle |\mu| \rangle^2 \quad (10)$$

The dielectric constants for the models are computed using eq 7 from simulations at 373 K and plotted against the average molecular dipole of the liquid in Figure 5. Consistent with eq 10, the data show a clear correlation between the size of the dipoles and the dielectric constant of the liquid. The data are most clearly distinguished by the type of electrostatic model employed. The models that have a molecular polarizability that resembles most closely the QM tensor (unscaled/vthole) give the best agreement with the experimental dielectric constant. Of note is the sensitivity of the dielectric constant to the size of the molecular dipole for this electrostatic model type. As a consequence, changes to the LJ parameters that give a modest change in the average dipole of the unscaled/vthole models ($\Delta$-$\langle |\mu| \rangle \approx 0.2$ Debye) can lead to dramatically different dielectric constants ($\Delta\varepsilon \approx 30$). The best dielectric model of this electrostatic class gives a value of $\varepsilon = 92 \pm 5$, in close agreement with the experimental value of 100 (see Tables 4 and 6). This Drude polarizable model will be used for subsequent calculations presented in this section.

There remains considerable uncertainty in determining appropriate parameters for polarizable force fields. At the simplest level, polarizabilities are presumed to be independent of environment. However, studies of the dispersion properties in crystals[70–73] and electronic structure calculations[84] have found a significant environmental impact on the atomic polarizabilities of halides. Ab initio studies have also found evidence for similar environmental effects on the polarizability of water.[85] Attempts to infer the environmental impact on water polarizability from empirical force field parametrizations have, however, been met with mixed results.[19,28,74] This suggests that, in part, the optimal polarizability may be sensitive to the details of empirical models. A possible explanation for observations of environmental effects argues that electron repulsion between neighboring molecules in the condensed phase can impede the electronic response of a molecule, effectively reducing

the molecular polarizability relative to the gas phase. The implication for a polarizable force field reduces to the selection of an appropriate model molecular polarizability. Model polarizabilities that capture the effective response in a liquid-like environment are the target, since the simulation of aqueous solvated biomolecules is the system of primary interest. In lieu of more direct quantitative assessments of effective molecular polarizabilities in condensed phase environments, we have chosen an empirical parametrization based on a bulk property that is sensitive to the polarized dipoles of the liquid; namely, the dielectric constant. Our results indicate that, for the amide molecules considered here, an appropriate model polarizability in the liquid corresponds well to the gas-phase value. This does not mean intermolecular electron repulsion effects do not play a role in this system. Simply put, such effects do not appear to impact significantly the polarizability of NMA when compared to the other parametrical features of the model.

Also included in Figure 5 is the data from a simulation of the nonpolarizable CHARMM model that gives $\langle|\mu|\rangle$ = 4.2 Debye and $\varepsilon = 37 \pm 2$. All polarizable models, regardless of electrostatic type, show a marked increase in the average molecular dipole and, consequently, in the dielectric constant compared with CHARMM. Fixed charge force fields attempt to capture the mean field response of a molecule to a condensed phase environment. In CHARMM, the amide dipole is 4.2 Debye, which is a 0.3 Debye increase relative to the dipole magnitude in the gas phase (3.9 Debye from QM). This is dramatically less than the average molecular dipole magnitude of 5.8 Debye corresponding to the Drude polarizable model at 308 K. Support for such a strong enhancement of the amide dipole comes from a recent Car–Parrinello (CP) simulation of liquid NMA,[86] in which the average molecular dipole magnitude is 6.0 Debye at the same temperature. This large difference in the amide dipole of polarizable relative to nonpolarizable models is also present in simulations of other polar environments. A simulation of dilute NMA solvated in water predicts an average dipole magnitude of 6.7 Debye, much larger than the 4.2 Debye dipole from the CHARMM force field. The poor representation of the mean field electrostatics in liquid NMA by the nonpolarizable model is not limited to the CHARMM force field. The amide dipole is 4.0 in OPLS/AA,[87] 4.4 in AMBER,[88] and 4.1 in GROMOS,[89] emphasizing that the phenomena may be an outcome of limitations in the form of the potential energy function.

The enhancement of the molecular dipoles alone does not fully explain the difference in the dielectric constant between the Drude and nonpolarizable models. The ratio of the dielectric constant between the Drude and CHARMM models is ≈40% larger than would be accounted for simply from the relative dipole magnitudes (see eq 10). Implied by this is that orientational ordering of the molecules in the polarizable model must be significantly greater than in the nonpolarizable model. Indeed, a direct measurement of this spatial correlation from the Kirkwood $G_K$ factor shows this to be the case. Table 3 gives the $G_K$ factors for the nonpolarizable CHARMM ($G_K = 3.0 \pm 0.2$) and polarizable Drude model ($G_K = 4.6 \pm 0.6$). The increased propensity for dipoles to align in the polarizable model can be understood by considering the driving force for these correlations: hydrogen bonding. In hydrogen-bonded configurations, the amide dipoles of constituent N-methylated amide molecules tend to align in parallel.[90–92] Stronger hydrogen bonds that arise from the enhanced dipole environment

of the polarizable Drude model stabilize to a greater extent configurations in which amide dipoles are aligned, manifesting in the large dielectric constant for this liquid.

The temperature dependence of this associativity can be inferred directly from experimental temperature-dependent dielectric data, since the molecular dipole moments are expected to vary weakly. The average dipole changes by ≈0.1 Debye between 308 and 373 K for the Drude model. In contrast, the dielectric constant is expected to drop precipitously with increasing temperature as the stabilizing contribution from hydrogen bonding is diminished in significance. This is observed experimentally when the dielectric constant drops from 170 at 308 K to 100 at 373 K.[11] Summarized in Table 4 are the dielectric constants for the Drude and CHARMM models corresponding to these temperatures. The experimental drop in the dielectric constant is adequately reproduced by the Drude polarizable model, which drops from 150 ± 15 at 308 to 92 ± 5 at 373K.

Dynamic properties that require the concerted breaking and reformation of hydrogen bonds are also expected to be sensitive to the inclusion of electrostatic polarization in the model. In the sub-nanosecond frequency range, experiments have found single exponential behavior for the dielectric relaxation of liquid NMA.[12,13] The associated time constant, termed the Debye time, is ≈700 ps at 308 K. This is very nearly 2 orders of magnitude longer than the room-temperature Debye time of liquid water (8.3 ps). From a molecular dynamics simulation, this time constant is related to an exponential fit to the system dipole autocorrelation function,[93]

$$\Phi(t) = \frac{\langle M(t) \bullet M(0) \rangle}{\langle M(0) \bullet M(0) \rangle} = e^{-t/\tau_D} \quad (11)$$

where $\tau_D$ is the Debye time. The exponential decay corresponding to experimental Debye times is plotted in Figure 6. Also included is the result from the Drude polarizable and nonpolarizable CHARMM models. The estimate from the polarizable model ($\tau_D$ = 660 ± 60 ps) is within the range of two experimental measurements: $\tau_D$ = 590 ps and $\tau_D$ = 740 ps.[12,13] The CHARMM model predicts a relaxation time that is five times too fast ($\tau_D$ = 140 ± 20 ps), consistent with the presumed relative weakness of hydrogen bonding in the liquid.

The relaxation time of the system dipole autocorrelation function provides an estimate for the simulation time that is required to generate independent samples of the system dipole (*M*). To accurately estimate the static dielectric constant from a molecular dynamics simulation, a sufficient sampling of *M* is required that will therefore depend on $\tau_D$. For the Drude model, total sampling time exceeded 50 ns to estimate properties related to the fluctuations of *M* (i.e, $\varepsilon$ and $G_K$). Recently, the static dielectric constant and Kirkwood $G_K$ factor of an ab initio liquid water model were estimated from a Car–Parrinello simulation[83,94] in which state-of-the-art simulation lengths extend to tens of picoseconds. A similar estimate from ab initio liquid NMA will require 2 orders of magnitude greater sampling.

### 3.3. Summary of NMA Properties

Gas-phase energetic properties of the Drude polarizable model of NMA are summarized alongside that of the nonpolarizable CHARMM model in Table 5. Included in the Table is the “best dielectric” Drude model (unscaled/vthole) and a representative of the scaled/vthole class of Drude models.

The configuration used to probe the NMA homodimer is illustrated in Figure 2. The interaction energy of the nonpolarizable model is found to be 1 kcal/mol too negative with respect to a high level QM calculation. This level of agreement is consistent with heterodimer energies of CHARMM NMA with TIP3P[95] water, which also overestimate the interaction strength by ~1 kcal/mol. This overestimation in the strength of dimer hydrogen bonding from nonpolarizable models is a consequence of an elevated model dipole that is meant to implicitly account for polarization effects from a polar condensed phase medium. In comparison, the polarizable molecule gives agreement to within 0.3 kcal/mol of the calculated QM dimer energy. The contrast of this result with the dielectric properties discussed in Section 3.2 is worth emphasizing. In gas-phase dimers, the hydrogen bonding interactions of the polarizable model are significantly weaker than in the nonpolarizable model. Even so, because of the explicit inclusion of polarizability, the Drude model gives rise to the strong molecular associations necessary to properly account for the anomalously large dielectric constant of liquid NMA, whereas the nonpolarizable model underestimates it by 70%.

The role of electronic polarization on the strength of these interactions can be shown in a simple example. The energy between an NMA monomer and the end of a chain of NMA molecules is compared for chains of varying length. The minimum energy along a selected intermolecular coordinate (illustrated in Figure 2) is plotted in Figure 7 for the CHARMM, Drude, and QM models. For a chain length of one NMA molecule, the intermolecular conformation corresponds to the NMA homodimer previously discussed in which the interaction energy of the Drude and QM models is ~1 kcal/mol less negative than that of the CHARMM model. As the chain length increases, the interaction energy becomes more negative for all three models due to attractive electrostatic interactions between the monomer and the other molecules in the chain. Eventually, the energy reaches a plateau as the contribution from molecules at the opposite end of the chain becomes small. Of note is the considerably larger increase in the interaction energy with increasing chain length for the Drude and QM models as compared to the fixed charge CHARMM model. For polarizable models, the attractive energy is strengthened not only by the additional molecules as the chain is lengthened but also by the cooperative increase in the magnitude of their dipoles. The increase in energy with increasing chain length of the Drude (unscaled/vthole) model accurately reproduces that of the QM model. In a water-solvated environment, the role played by electronic polarization is expected to be more pronounced than these gas-phase cluster calculations. The inset to Figure 7 gives the dipole magnitude of the NMA monomer that interacts with the NMA chain. The dipole of the unscaled/vthole Drude model plateaus at a value of 4.8 Debye, considerably less than the average dipole observed in neat NMA (5.7 Debye) or hydrated NMA (6.7 Debye). Even so, the contribution to the energy from electronic polarization is significant enough for the unscaled/vthole Drude and QM models

to surpass the CHARMM energy for chain lengths greater than three NMA molecules. The role played by such cooperative effects in hydrogen-bonding networks of peptides has been studied recently using ab initio methods,[96,97] and it will be of some interest to explore this and basic issues regarding the impact of moving from a nonpolarizable to a polarizable protein force field on the relative stability of secondary structural elements that form such hydrogen-bonding networks as protein helices and sheets.

In addition to the target data used to select the best models, Table 6 includes the hydration free energy of NMA and dynamic properties, including the Debye relaxation time and the self-diffusion constant of liquid NMA. Both the CHARMM and Drude (scaled/vthole) models overestimate the self-diffusion and underestimate the Debye relaxation time, consistent with the decreased hydrogen bonding in the condensed phase, as discussed above; the Drude (unscaled/vthole) model is in good agreement with experiment. This trend in the hydrogen-bonding strength of the models is evident in the condensed phase energetic properties, as well. The energetics are strongest for the unscaled/vthole Drude model, followed by the scaled/vthole Drude model and the fixed charge CHARMM model. Owing to the lack of consistency in the experimental estimates for the enthalpy of vaporization,[77,78] it is difficult to draw conclusions regarding the fidelity of the models with respect to this property. Regarding the hydration free energy, the unscaled/vthole Drude model appears to be somewhat too favorable; however, as mentioned in Section 3.1, Lennard-Jones parameters associated with the methyl groups have not been part of the present parametrization, in which standard aliphatic parameters[23] have been used to limit the parameter space search. Preliminary tests indicate that modest changes in the aliphatic Lennard-Jones parameters can lead to more optimal unscaled/vthole models that give hydration free energies consistent with experiment while not compromising the other properties studied in this report. With the exception of the dielectric properties, all three models are in satisfactory agreement for many of the condensed phase properties.

### 3.4. The Amide Series

Experiments have shown a definitive relationship between methyl substitutions of amide molecules and their dielectric properties.[12] N-Methylated amides are found to have anomalously large dielectric constants, whereas unsubstituted amides have dielectric constants of intermediate size, and N,N-dimethylated amides have the smallest dielectric constants. To explore this trend, Drude polarizable models of acetamide and *N*,*N*-dimethyl acetamide are parametrized. Table 8 summarizes the gas-phase electrostatic and dielectric properties for these amides along with the Drude polarizable model of NMA. There is no simple relationship between monomer electrostatics and the dielectric constant for these amide liquids. The dielectric behavior can, however, be explained in terms of hydrogen bonding. The small dielectric constant for N,N-dimethylated amides is clearly a consequence of the lack of an available polar hydrogen atom that can associate with a neighbor's carbonyl oxygen. The experimental dielectric constant of liquid *N*,*N*-dimethyl acetamide for the Drude model is 23, in close correspondence to the experimental value of 26. This lack of hydrogen bonding also affects the degree of induced polarization in the molecule relative to the other amides. The average dipole of *N*,*N*-dimethyl acetamide (5.0 Debye) is considerably smaller than the ≈5.8 Debye average dipole of the other two amide

liquids. The average magnitude of the molecular dipole from Car–Parrinello simulations of these amide liquids is also included in Table 8, which compares well with the Drude models. Somewhat surprising is the similar average dipole of acetamide and NMA, even though the dielectric constant of liquid acetamide is two-thirds the magnitude of liquid NMA. The smaller dielectric constant of unsubstituted amides as compared to their N-methylated counterparts have been rationalized by geometric considerations. Figure 8 illustrates the parallel alignment of amide dipoles when an NMA molecule has two hydrogen-bonding partners. In contrast, hydrogen bonds can form with both the cis and trans hydrogens of acetamide. Hydrogen bonds that form to the cis hydrogen of acetamide lead to anticorrelated amide dipoles, as shown in Figure 8. This orientational ordering in hydrogen-bonding configurations is reflected in the Kirkwood $G_K$ factor of liquid acetamide ($G_K = 2.4 \pm 0.2$), which is approximately one-half that of NMA.

### 3.5. Conclusions

Simulations involving quantum mechanical ab initio models can provide valuable insight into molecular condensed phase properties; however, the extensive computational time necessary to resolve bulk properties makes it difficult to validate the fidelity and thus properly assess the impact of such models. For computationally simpler models based on a parametrized potential function, a full exploration of the bulk-phase properties is achievable. Although the parameters of these models can be freely adjusted to reproduce any individual property, the structure of the potential function restricts the possible candidates that will agree with the aggregate of available molecular properties. Although such constraints are certainly model-specific, they do qualitatively reflect important trends that are inherent to the physics of these molecular systems.

To investigate the sensitivity that properties of *N*-methyl acetamide have on the magnitude and orientation of the model molecular polarizability, four classes of electrostatic Drude model were studied. Each class required a complimentary set of Lennard-Jones parameters found through an exhaustive search in the space of LJ parameters. Candidate LJ parameters were selected on the basis of how well they compare to available QM and experimental data for a suite of model properties that includes gas phase interactions with water and properties that probe the molecular volume, energetic, and dielectric properties in the condensed phase. The results suggest that the aforementioned magnitude and orientation of the gas-phase molecular polarizability play an important role in determining a model that adequately accounts for the properties of NMA; in particular, the dielectric properties. In the final analysis, it is the model that gives a magnitude and orientation of the molecular polarizability in the closest correspondence to high-level gas phase ab initio data that gives molecular properties that best agree with experiment.

The polarizable Drude model predicts an average molecular dipole of 5.7 Debye in neat liquid NMA, significantly larger than that of available fixed charge models 4.0–4.4 Debye and consistent with that found in Car–Parrinello simulations. The large magnitude of the average molecular dipole in the polarizable model of liquid NMA leads to greater orientational ordering. Taken together, these two characteristics have been shown to account for the anomalously large dielectric constant of liquid NMA. Moreover, it has been

demonstrated how the disruption in liquid ordering with increasing temperature accounts for the temperature dependence of $\varepsilon(T)$, even while the average molecular dipole remains approximately constant. The strong interactions associated with these large dipoles result in slower dynamic properties relative to a nonpolarizable model. The Drude model of liquid NMA predicts a Debye relaxation time that is consistent with experiments, whereas the nonpolarizable CHARMM model predicts a relaxation time that is ~5 times too fast. Polarizable models for acetamide and *N*,*N*-dimethyl acetamide were also parametrized. The polarizable models give good agreement with the dielectric constants of this series, which range from the small (*N*,*N*-dimethyl acetamide) the intermediate (acetamide) to the large (NMA).

Motivating the present work is an effort to build an accurate and reliable polarizable force field for proteins. As a molecular analog to the amidelike units that constitute the polypeptide backbone of proteins, assessing the parametrical features necessary to accurately model NMA is a critical step toward determining appropriate parameters for proteins. The present study has illustrated how careful addition of explicit electrostatic polarizability to a model can lead to greater accuracy in properties sensitive to the intermolecular associativity of amide molecules arising from hydrogen bonding, properties include the liquid dielectric constant, Debye relaxation time, and diffusion constant. Further, the model is able to capture cooperative electronic effects that contribute to the interaction energy of hydrogen bonding, represented here by the interaction of an NMA monomer with a chain of NMA molecules of variable length, properties poorly represented by traditional fixed charge force fields. Similar interamide hydrogen bonding also plays a crucial role in the secondary structure elements of proteins, including sheets and helices. We anticipate that greater accuracy in modeling such hydrogen bonding interactions by including explicit electrostatic polarization may lead to a more faithful representation of the relative stability of these secondary structure elements.

## Supplementary Material

Refer to Web version on PubMed Central for supplementary material.

## Acknowledgment

Financial support to A.D.M. is acknowledged from the NIH (GM 51501) and to B.R. and A.D.M. from the NIH (GM 072558). Computer time allocations were received from DOD ACS Major Shared Resource Computing and PSC Pittsburgh Supercomputing Center. E.H. thanks Yuqing Deng for help with the free energy simulations.

## References and Notes

1. MacKerell AD Jr. Bashford D, Bellott M, Dunbrack RL Jr. Evanseck JD, Field MJ, Fisher S, Gao J, Guo H, Ha S, Joseph-McCarthy D, Kuchnir L, Kuczera K, Lau FTK, Mattos C, Michnick S, Ngo T, Nguyen DT, Prodhorn B, Reiher WE III, Roux B, Schlenkrich M, Smith JC, Stote R, Straub J, Watanabe M, Wirkiewicz-Kuczera D, Yin D, Karplus M. J. Phys. Chem. B. 1998; 102:3586–3616. [PubMed: 24889800]
2. Jorgensen WL, Maxwell DS, Tirado-Rives J. J. Am. Chem. Soc. 1996; 118:11225–11236.
3. Cornell WD, Cieplak P, Bayly CI, Gould IR Jr. Merz KM, Ferguson DM, Spellmeyer DC, Fox T, Caldwell JW, Kollman PA. J. Am. Chem. Soc. 1995; 117:5179–5197.

4. van Gunsteren, WF.; Billeter, SR.; Eising, AA.; Huenenberger, PH.; Krueger, P.; Mark, AE.; Scott, WRP.; Tironi, IG. Biomolecular Simulation: The GROMOS96 Manual and User Guide. Hochshulverlag AG/ETH; Zurich: 1996.
5. Srinivasan R, Rose GD. Proc. Natl. Acad. Sci. 1999; 96:14258–14263. [PubMed: 10588693]
6. Zhou RH, Berne BJ, Germain R. Proc. Natl. Acad. Sci. 2001; 98:14931–14936. [PubMed: 11752441]
7. Garcia AE, Sonbonmatsu KY. Proteins Struct. Funct. Genet. 2001; 42:345–354. [PubMed: 11151006]
8. Bolhuis PG. Proc. Natl. Acad. Sci. 2003; 100:12129–12134. [PubMed: 14523242]
9. Sheridan RP, Lee RH, Peters N, Allen LC. Biopolymers. 1979; 18:2451–2458.
10. Lutskii AE, Mikhailenko SA. Zh. Strukt. Khim. 1962; 4:323–325.
11. Lin R-Y, Dannhauser WJ. Am. Chem. Soc. 1963; 67:1805–1810.
12. Bass SJ, Nathan WI, Meighan RM, Cole RH. J. Phys. Chem. 1964; 68:509–515.
13. Omar MM. J. Chem. Soc. Faraday Trans. 1980; 76:711–716.
14. Barthel J, Buchner R, Wurm BJ. Mol. Liq. 2002; 98-99:51–69.
15. Barthel J, Bachhuber K, Buchner R, Gill JB, Kleebauer M. Chem. Phys. Lett. 1990; 167:62–66.
16. Kirkwood JG. J. Chem. Phys. 1939; 7:911.
17. Whitfield TW, Martyna GJ, Allison S, Bates SP, Vass H, Crain J. J. Phys. Chem. B. 2006; 110:3624–3637. [PubMed: 16494418]
18. Essex JW, Jorgensen WL. J. Phys. Chem. 1995; 99:17956–17962.
19. Lamoureux G, MacKerell AD Jr. Roux B. J. Chem. Phys. 2003; 119:5185–5197.
20. Lamoureux G, Harder E, Vorobyov IV, Roux B, MacKerell AD Jr. Chem. Phys. Lett. 2006; 418:245–249.
21. Anisimov VM, Lamoureux G, Vorobyov I, Huang N, Roux B, MacKerell AD Jr. J. Chem. Theory Comput. 2005; 1:153–168. [PubMed: 26641126]
22. Harder E, Anisimov VM, Vorobyov IV, Lopes PEM, Noskov SY, MacKerell AD Jr. Roux B. 2006; 2:1587–1597.
23. Vorobyov IV, Anisimov VM, MacKerell AD Jr. J. Phys. Chem. B. 2005; 109:18988–18999. [PubMed: 16853445]
24. Lopes PEM, Lamoureux G, Roux B, MacKerell AD Jr. J. Phys. Chem. B. 2007; 111:2873–2885. [PubMed: 17388420]
25. Vorobyov I, Anisimov VM, Greene S, Venable RM, Moser A, Pastor RW, MacKerell AD Jr. 2007; 3:1120–1133.
26. Lamoureux G, Roux B. J. Phys. Chem. B. 2006; 110:3308–3322. [PubMed: 16494345]
27. Anisimov VM, Vorobyov IV, Roux B, MacKerell AD Jr. J. Chem. Theory and Comput. 2007; 3:1927–1946. [PubMed: 18802495]
28. Stern HA, Berne BJ, Friesner RA. J. Chem. Phys. 2001; 115:2237–2251.
29. Thole BT. Chem. Phys. 1981; 59:341–350.
30. Banks JL, Kaminski GA, Zhou R, Mainz DT, Berne BJ, Friesner RA. J. Chem. Phys. 1999; 110:741–754.
31. Stern HA, Kaminski GA, Banks JL, Zhou R, Berne BJ, Friesner RA. J. Phys. Chem. B. 1999; 103:4730–4737.
32. Liu Y-P, Kim K, Berne BJ, Friesner RA, Rick SW. J. Chem. Phys. 1998; 108:4739–4755.
33. Kaminski GA, Stern HA, Berne BJ, Friesner RA, Cao YX, Murphy RB, Zhou R, Halgren TA. J. Comp. Chem. 2002; 23:1515–1531. [PubMed: 12395421]
34. Becke AD. Phys. Rev. A: At., Mol., Opt. Phys. 1988; 38:3098–3100.
35. Lee C, Yang W, Parr RG. Phys. Rev. B: Condens. Matter Mater. Phys. 1988; 37:785–789.
36. Allen FH. Acta Crystallogr., B. 2002; 58:370–379. [PubMed: 12037358]
37. Herrebout WA. J. Phys. Chem. A. 2001; 105:4865–4881.
38. Drakenberg T, Forsen S. Chem. Commun. 1971:1404.

39. Frisch, MJ.; Trucks, GW.; Schlegel, HB.; Scuseria, GE.; Robb, MA.; Cheeseman, JR.; Montgomery, JA., Jr.; Vreven, T.; Kudin, KN.; Burant, JC.; Millam, JM.; Iyengar, SS.; Tomasi, J.; Barone, V.; Mennucci, B.; Cossi, M.; Scalmani, G.; Rega, N.; Petersson, GA.; Nakatsuji, H.; Hada, M.; Ehara, M.; Toyota, K.; Fukuda, R.; Hasegawa, J.; Ishida, M.; Nakajima, T.; Honda, Y.; Kitao, O.; Nakai, H.; Klene, M.; Li, X.; Knox, JE.; Hratchian, HP.; Cross, JB.; Bakken, V.; Adamo, C.; Jaramillo, J.; Gomperts, R.; Stratmann, RE.; Yazyev, O.; Austin, AJ.; Cammi, R.; Pomelli, C.; Ochterski, JW.; Ayala, PY.; Morokuma, K.; Voth, GA.; Salvador, P.; Dannenberg, JJ.; Zakrzewski, VG.; Dapprich, S.; Daniels, AD.; Strain, MC.; Farkas, O.; Malick, DK.; Rabuck, AD.; Raghavachari, K.; Foresman, JB.; Ortiz, JV.; Cui, Q.; Baboul, AG.; Clifford, S.; Cioslowski, J.; Stefanov, BB.; Liu, G.; Liashenko, A.; Piskorz, P.; Komaromi, I.; Martin, RL.; Fox, DJ.; Keith, T.; Al-Laham, MA.; Peng, CY.; Nanayakkara, A.; Challacombe, M.; Gill, PMW.; Johnson, B.; Chen, W.; Wong, MW.; Gonzalez, C.; Pople, JA. Gaussian 03, revision C.02. Gaussian, Inc.; Wallingford, CT: 2004.
40. Scott PA, Radom L. J. Phys. Chem. 1996; 100:16502–16513.
41. Kuczera K, Wiorkiewiez-Kuczera J, Karplus M. MOLVIB program.
42. Pulay P. J. Am. Chem. Soc. 1979; 101:2550–2560.
43. Brooks BR, Bruccoleri RE, Olafson BD, States DJ, Swaminathan S, Karplus M. J. Comput. Chem. 1983; 4:187–217.
44. MacKerell, AD., Jr.; Brooks, B.; Brooks, CB., III; Nilsson, L.; Roux, B.; Won, Y.; Karplus, M. Encyclopedia of Computational Chemistry. Vol. 1. John Wiley & Sons; Chichester: 1998. CHARMM: The Energy Function and Its Parameterization with an Overview of the Program..
45. Boys S-F, Bernardi F. Mol. Phys. 2002; 100:65–73.
46. Shao Y, Fusti-Molnar L, Jung Y, Kussmann J, Ochsenfeld C, Brown ST, Gilbert AT, Slipchenko LV, Levchenko SV, O'Neill DP, DiStasio RA Jr. Lochan RC, Wang T, Beran GJO, Besley NA, Herbert JM, Lin CY, Voorhis TV, Chien SH, Sodt A, Steele RP, Rassolov VA, Maslen PE, Korambath PP, Adamson RD, Austin B, Baker J, Byrd EFC, Daschel H, Doerksen RJ, Dreuw A, Dunietz BD, Dutoi AD, Furlani TR, Gwaltney SR, Heyden A, Hirata S, Hsu C-P, Kedziora G, Khalliulin RZ, Klunzinger P, Lee AM, Lee MS, Liang W, Lotan I, Nair N, Peters B, Proynov EI, Pieniazek PA, Rhee YM, Ritchie J, Rosta E, Sherrill CD, Simmonett AC, Subotnik JE, Woodcock HL III, Zhang W, Bell AT, Chakraborty AK, Chipman DM, Keil FJ, Warshel A, Hehre WJ, Schaefer HF III, Kong J, Krylov AI, Gill PM, Head-Gordon M. Phys. Chem. Chem. Phys. 2006; 8:3172–3191. [PubMed: 16902710]
47. Feyereisen M, Fitzgerald G, Komornicki A. Chem. Phys. Lett. 1993; 208:359–363.
48. Weigend F, Haser M. Theor. Chem. Acc. 1997; 97:331–340.
49. Allen, MP.; Tildesley, DJ. Computer Simulation of Liquids. Oxford University Press, Inc.; New York: 1987.
50. Martyna GJ, Klein ML, Tuckerman M. J. Chem. Phys. 1992; 97:2635–2643.
51. Martyna GJ, Tobias DJ, Klein ML. J. Chem. Phys. 1994; 101:4177.
52. Martyna GJ, Tuckerman ME, Tobias DJ, Klein ML. Mol. Phys. 1996; 87:1117–1157.
53. Andersen HC. J. Comput. Phys. 1983; 52:24.
54. Harder E, Kim B, Friesner RA, Berne BJ. J. Chem. Theory Comput. 2005; 1:169. [PubMed: 26641127]
55. Lamoureux G, Roux B. J. Chem. Phys. 2003; 119:3025–3039.
56. Essmann U, Perera L, Berkowitz ML, Darden T, Lee H, Pedersen LG. J. Chem. Phys. 1995; 103:8577.
57. Weeks JD, Chandler D, Andersen HC. J. Chem. Phys. 1971; 54:5237–5247.
58. Deng Y, Roux B. J. Phys. Chem. B. 2004; 108:16567–16576.
59. Samuelson S, Martyna GJ. Chem. Phys. 1998; 109:11061–11073.
60. Tuckerman ME, Yarne D, Samuelson SO, Hughes AL, Martyna G. J. Comput. Phys. Commun. 2000; 128:333–376.
61. Troullier N, Martins JL. Phys. Rev. B: Condens. Matter Mater. Phys. 1991; 43:1993–2006.
62. Tassone F, Mauri F, Car R. 1994; 50(15):10561–10573.
63. Tuckerman ME, Parrinello MJ. Chem. Phys. 1994; 101:1302–1315.

64. Tuckerman ME, Parrinello MJ. Chem. Phys. 1994; 101:1316–1329.
65. Hutter J, Tuckerman ME, Parrinello MJ. Chem. Phys. 1995; 102:859–871.
66. Martyna GJ, Tuckerman ME, Tobias DJ, Klein ML. Mol. Phys. 1996; 87:1117–1157.
67. Wannier GH. Phys. Rev. 1937; 52:191–197.
68. Foster JM, Boys SF. Rev. Mod. Phys. 1960; 32:300–302.
69. Resta R, Sorella S. Phys. Rev. Lett. 1999; 82:370–373.
70. Coker H. J. Phys. Chem. 1976; 80:2078.
71. Mahan GD. J. Chem. Phys. 1982; 76:493.
72. Fowler PW, Madden PA. Phys. Rev. B: Condens. Matter Mater. Phys. 1984; 29:1035.
73. Jemmer P, Fowler PW, Wilson M, Madden PA. J. Phys. Chem. A. 1998; 102:8377.
74. Ren P, Ponder JW. J. Phys. Chem. B. 2003; 107:5933–5947.
75. Harder E, Eaves JD, Tokmakoff A, Berne BJ. Proc. Natl. Acad. Sci. 2005; 102:11611–11616. [PubMed: 16081533]
76. Ren P, Ponder JW. J. Comput. Chem. 2002; 23:1497–1506. [PubMed: 12395419]
77. Aucejo J, Montón JB, Muñoz R, Sanchotello M. J. Chem. Eng. Data. 1993; 38:160–162.
78. Manczinger J, Kortum G. Z. Phys. Chem. 1975; 95:177–186.
79. Deutch JM. Annu. Rev. Phys. Chem. 1973; 24:301–323.
80. de Leeuw SW, Perram JW, Smith ER. Annu. Rev. Phys. Chem. 1986; 37:245–270. [PubMed: 21819241]
81. Neumann M, Steinhauser O. Chem. Phys. Lett. 1984; 106:563–569.
82. Hochtl P, Boresch S, Bitomsky W, Steinhauser O. J. Chem. Phys. 1988; 109:4927–4937.
83. Sharma M, Resta R, Car R. Phys. Rev. Lett. 2007; 98:247401. [PubMed: 17677991]
84. Valderrama E, Wheatley RJ. 2003; 24:2075–2082.
85. Morita A. 2002; 23:1466–1471.
86. Whitfield TW, Crain J, Martyna GJ. J. Chem. Phys. 2006; 124:094503.
87. Kaminski G, Jorgensen WL. J. Phys. Chem. 1996; 100:18010–18013.
88. Caldwell JW, Kollman PA. J. Phys. Chem. 1995; 99:6208–6219.
89. Hermans J, Berendsen HJC, van Gunsteren WF, Postma JPM. Biopolymers. 1984; 23:1513–1518.
90. Trabelsi S, Bahri M, Nasr S. J. Chem. Phys. 2005; 122:024502. [PubMed: 15638593]
91. Vargas R, Garza J, Friesner RA, Stern H, Hay BP, Dixon DA. J. Phys. Chem. A. 2001; 105:4963–4968.
92. Dixon DA, Dobbs KD, Valentini JJ. J. Phys. Chem. 1994; 98:13435–13439.
93. Rick SW, Stuart SJ, Berne BJ. J. Chem. Phys. 1994; 101:6141–6156.
94. Silvistrelli PL, Parrinello M. J. Chem. Phys. 1999; 111:3572–3580.
95. Jorgensen WL, Chandrasekhar J, Madura JD, Impey RW, Klein ML. J. Chem. Phys. 1983; 79:926–935.
96. Parker LL, Houk AR, Jensen JH. J. Am. Chem. Soc. 2006; 128:9863–9872. [PubMed: 16866544]
97. Wieczorek R, Dannenberg JJ. J. Am. Chem. Soc. 2005; 127:17216–17223. [PubMed: 16332068]
98. Boje L, Hvidt A. J. Chem. Thermodyn. 1971; 3:663–673.
99. Wolfenden R. Biochemistry. 1978; 17:201–204. [PubMed: 618544]
100. Chen LP, Gross T, Ludemann HD. Z. Phys. Chem. 2000; 214:239–251.
101. Williams WD, Ellard JA, Dawson LR. J. Am. Chem. Soc. 1952; 79:4652–4654.
102. Yeh I-C, Hummer G. J. Phys. Chem. B. 2004; 108:15873–15879.
103. Chickos JS, Acree WE Jr. J. Phys. Chem. Ref. Data. 2003; 32:519–878.

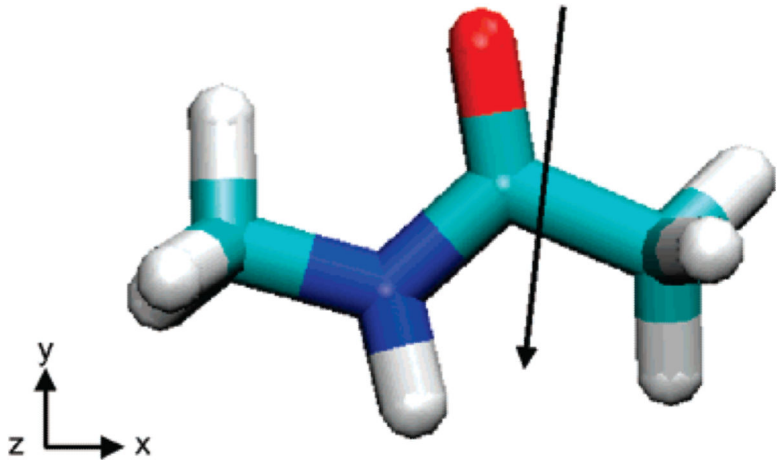


**Figure 1.**

Orientation of NMA monomer used to characterize the gas-phase electrostatic properties. The arrow represents the direction of the molecular dipole from a QM calculation at the B3LYP/aug-cc-pVDZ level.

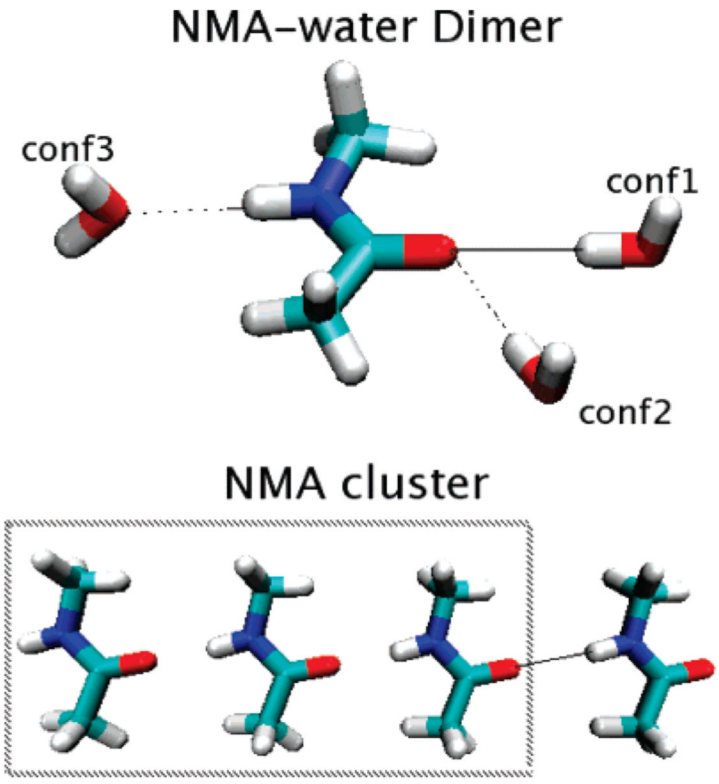


**Figure 2.**

Illustrated are the three conformations used to calculate the interaction energy for heterodimers of NMA with water. Also included is the configuration used to calculate the interaction energy between a molecule of NMA and a chain of NMA molecules. The illustrated box shows a chain of three NMA molecules. The configuration used to evaluate the energy of the NMA homodimer corresponds to a chain length of one NMA molecule.

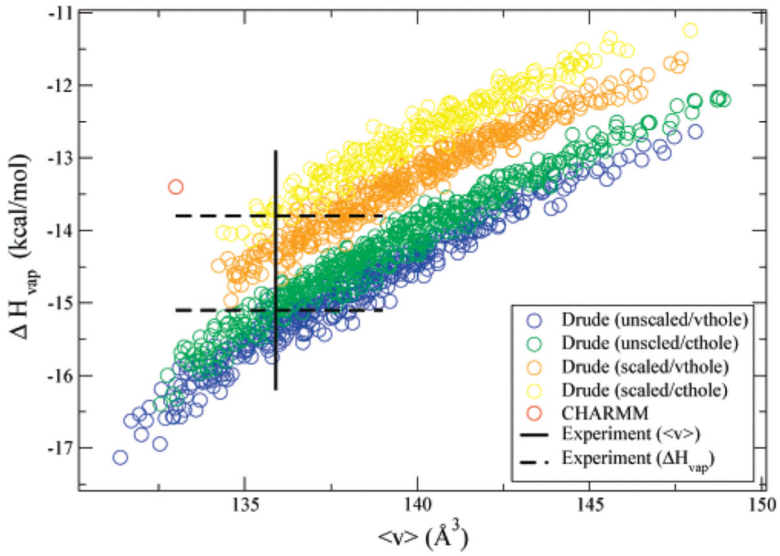


**Figure 3.**

The enthalpy of vaporization and molecular volume of neat liquid simulations for the four electrostatic models studied. Also included is the nonpolarizable CHARMM model. The simulations were run at $T$ = 373 K. Each electrostatic model corresponds to a color. The individual circles of each electrostatic model type correspond to a different choice of LJ parameters. Each model gives interaction energies and geometries that agree to within 0.5 kcal/mol and 0.15 Å of QM calculations for the NMA–water dimer optimizations illustrated in Figure 2. The enthalpy of vaporization is calculated from the average change in energy upon formation of the dense system, $\Delta H_{vap} = kT - (\langle u \rangle_{liq} - \langle u \rangle_{gas})$. Models that lie within 0.5 Å$^3$ of the experimental molar volume (black box) were chosen for the next stage of the parametrization. Two estimates for the experimental enthalpy are illustrated.[77,78]

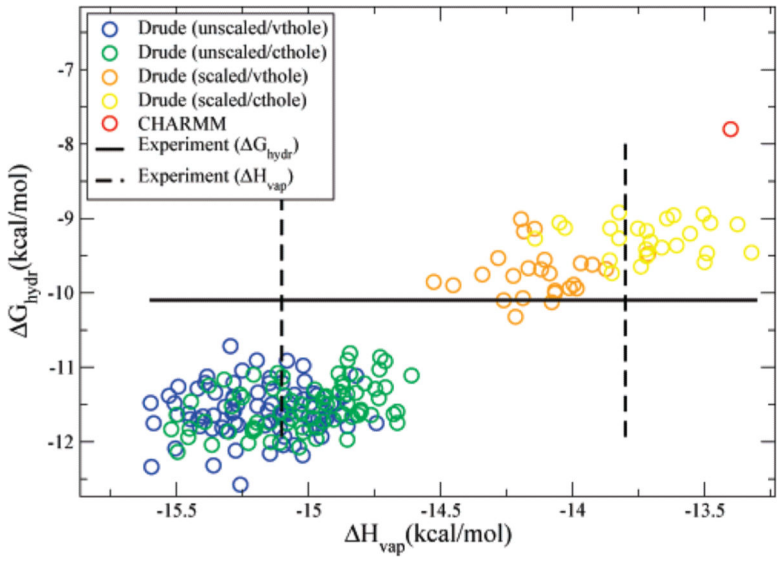


**Figure 4.**

The hydration free energy and enthalpy of vaporization of the neat liquid for the four electrostatic models studied. Also included is the nonpolarizable CHARMM model. The neat liquid simulations were run at $T$ = 373 K. The hydration free energy data corresponds to $T$ = 298 K. Each electrostatic model corresponds to a color. The individual circles of each electrostatic model type correspond to a different choice of LJ parameters. Each model gives interaction energies and geometries that agree to within 0.5 kcal/mol and 0.15 Å of QM calculations for the NMA–water dimer optimizations illustrated in Figure 2 and is within 1% of the experimental neat liquid molecular volume. Two estimates for the experimental enthalpy are illustrated.[77,78]

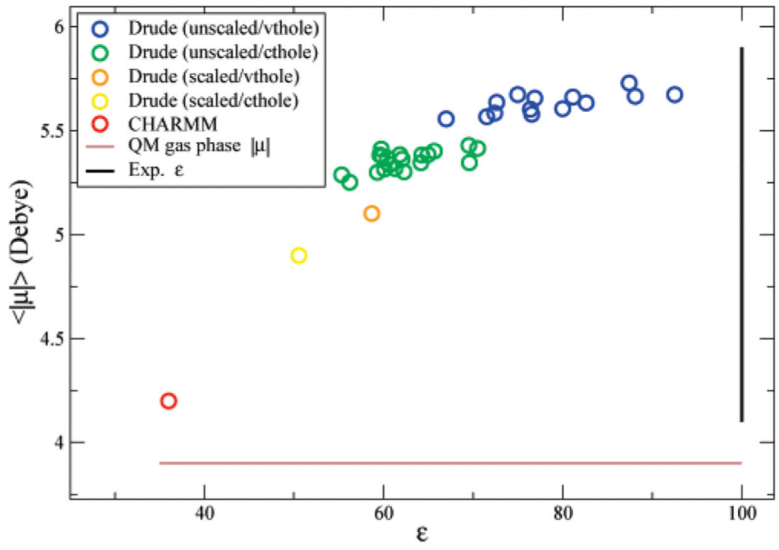


**Figure 5.**

The static dielectric constant with the average molecular dipole calculated from neat liquid simulations for the four electrostatic models studied. Also included is the nonpolarizable CHARMM model. The simulations were run at $T$ = 373 K. Each electrostatic model corresponds to a color. The individual circles of each electrostatic model type correspond to a different choice of LJ parameters. The models were selected to give satisfactory agreement with QM data for water dimer data as well as the molecular volume in liquid NMA and the hydration free energy. The experimental dielectric constant and QM gas-phase dipole of NMA at the B3LYP/aug-cc-pVDZ level are also represented by solid black and brown lines, respectively.

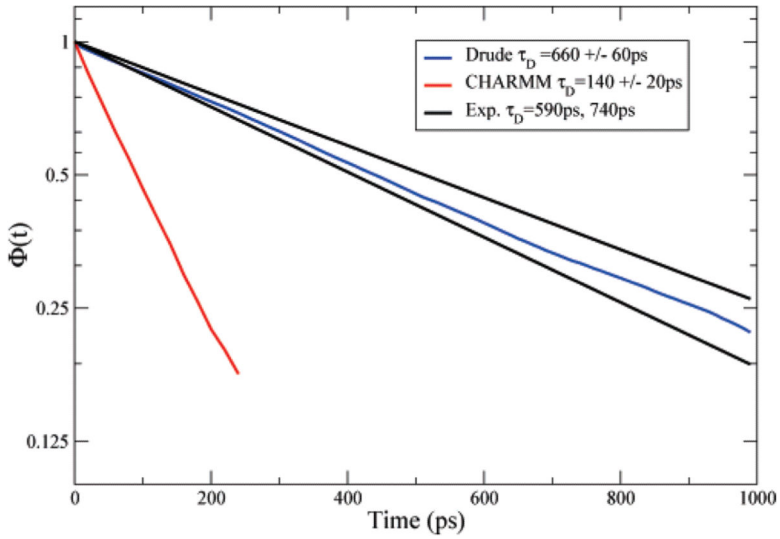


**Figure 6.**

The autocorrelation function of the system dipole, $M(t)$, plotted on a semilog plot. The Debye relaxation time ( $\tau_D$) is extracted from a single-exponential fit. The simulations and experiment correspond to a temperature of $T$ = 308 K. The experimental curves correspond to single exponentials with a time constant corresponding to the experimental Debye time. The Drude model corresponds to the optimal choice of LJ parameters from the unscaled/vthole class of electrostatic models.

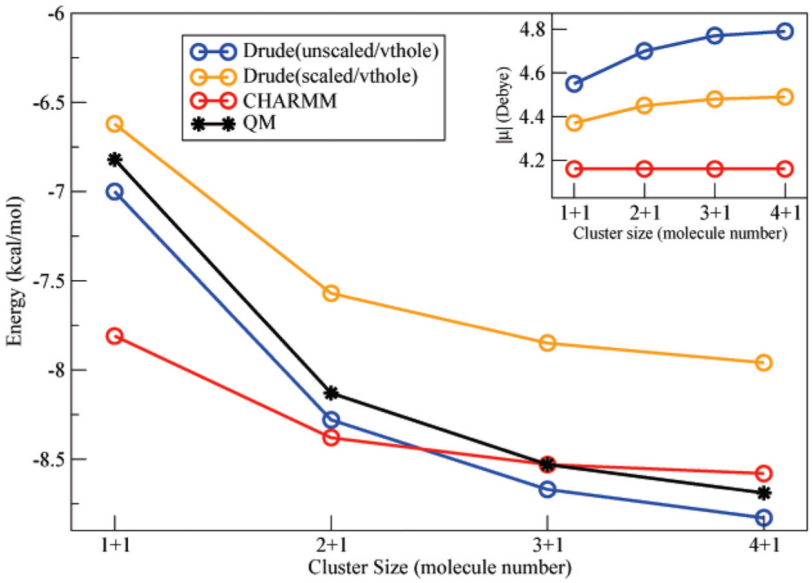


**Figure 7.**

The interaction energy between a monomer of NMA with small clusters of NMA in chainlike configurations (see Figure 2) is plotted against the cluster size. The cluster size (*x* + 1) includes a chain of *x* number of NMA molecules and an interacting monomer. The energies correspond to the minimum along the radial coordinate illustrated in Figure 2. The QM energies are computed at the RI-MP2/6-311+G(3df,2p) level from minimized configurations at the MP2/6-31G(d) level.

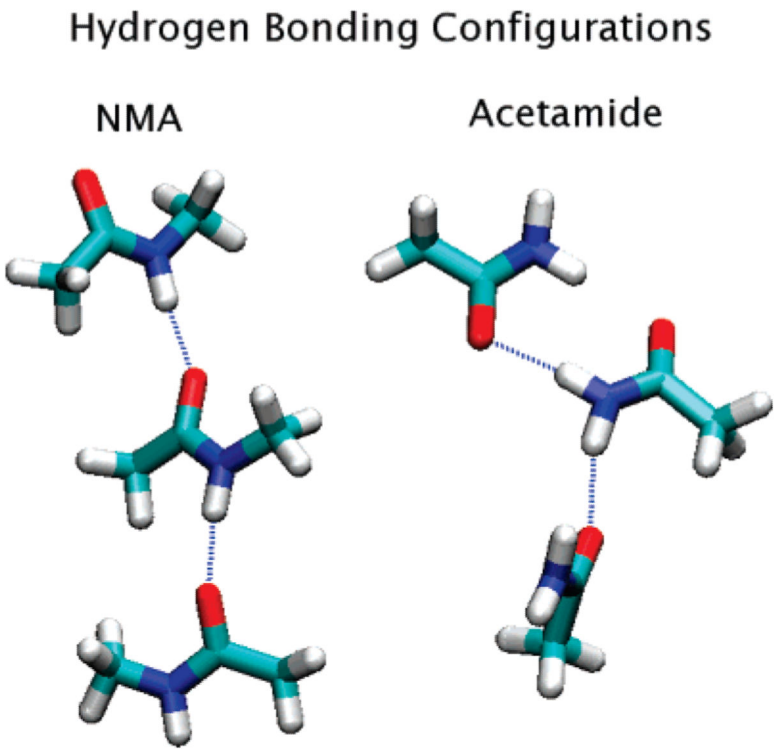


**Figure 8.**

Representative configurations from a neat liquid simulation of NMA and acetamide. Illustrated is the chainlike configurations found in liquid NMA and ringlike configurations found in acetamide.

## TABLE 1

The Molecular Dipole of NMA[a]

| dipole | QM | Drude (unscaled/vthole) | Drude (unscaled/cthole) | Drude (scaled/vthole) | Drude (scaled/cthole) |
|---|---|---|---|---|---|
| $\mu_x$ | 0.36 | 0.35 | 0.51 | 0.83 | 1.08 |
| $\mu_y$ | 3.89 | 3.84 | 3.86 | 3.80 | 3.74 |
| $\mu_z$ | 0.06 | 0.0 | 0.0 | 0.0 | 0.0 |
| $\mu$ | 3.9 | 3.9 | 3.9 | 3.9 | 3.9 |

[a]The QM dipole is calculated using density functional theory at the B3LYP/aug-cc-pVDZ level. The table includes four electrostatic Drude models, which are distinguished by the magnitude and orientation of their polarizability tensor (see text for definitions). The orientation of the monomer with respect to the Cartesian axes is illustrated in Figure 1.

## TABLE 2

Molecular Polarizabilities of NMA[a]

| $\bar{\alpha}$ | QM | Drude (unscaled/vthole) | Drude (unscaled/cthole) | Drude (scaled/vthole) | Drude (scaled/cthole) |
|---|---|---|---|---|---|
| $\alpha_{xx}$ | 9.4 | 9.2 | 13.0 | 6.5 | 8.2 |
| $\alpha_{xy}$ | 0.4 | 0.6 | 0.0 | 0.4 | 0.0 |
| $\alpha_{xz}$ | 0.0 | 0.0 | 0.0 | 0.0 | 0.0 |
| $\alpha_{yy}$ | 8.0 | 8.0 | 6.8 | 5.8 | 4.9 |
| $\alpha_{yz}$ | 0.0 | 0.0 | 0.0 | 0.0 | 0.0 |
| $\alpha_{zz}$ | 6.0 | 6.4 | 5.0 | 4.7 | 3.7 |
| $\frac{1}{3}$TR($\bar{\alpha}$) | 7.8 | 7.9 | 8.3 | 5.7 | 5.6 |

[a]The QM tensor is calculated using density functional theory at the B3LYP/aug-cc-pVDZ basis level. The table includes four electrostatic Drude models, which are distinguished by the magnitude and orientation of their polarizability tensor (see text for definitions). The orientation of the monomer with respect to the Cartesian axes is illustrated in Figure 1.

## TABLE 3

The Kirkwood $G_K$ Factor Computed from Neat Liquid NMA Simulations at 373 K[a]

| NMA | $G_K$ |
|---|---|
| Drude | 4.6 ± 0.6 |
| CHARMM | 3.0 ± 0.2 |

[a]The Drude model corresponds to the optimal choice of LJ parameters from the unscaled/vthole class of electrostatic models.

## TABLE 4

The Temperature Dependence of the Dielectric Constant from Simulations at 308 and 373 K[a]

| NMA | $\varepsilon$ ($T$ = 308 K) | $\varepsilon$ ($T$ = 373 K) |
|---|---|---|
| experiment | 170 | 100 |
| Drude | 150 ± 15 | 92 ± 5 |
| CHARMM | 55 ± 5 | 37 ± 2 |

[a]The Drude model corresponds to the optimal choice of LJ parameters from the unscaled/vthole class of electrostatic models.

**TABLE 5**

Summary of Drude Polarizable and CHARMM NMA Gas-Phase Dimer Interaction Energies for Heterodimers of NMA with Water and an NMA–NMA Homodimer[a]

| properties | experiment/QM kcal/mol | CHARMM kcal/mol | Drude (unscaled/vthole) kcal/mol | Drude (scaled/vthole) kcal/mol |
|---|---|---|---|---|
| $E_{min}$ (NMA–water: conf1) | –5.3 | –6.6 | –5.5 | –5.6 |
| $E_{min}$ (NMA–water: conf2) | –6.3 | –6.2 | –6.3 | –6.5 |
| $E_{min}$ (NMA–water: conf3) | –4.7 | –6.4 | –5.0 | –4.7 |
| $E_{min}$ (NMA–NMA: dimer) | –6.8 | –7.8 | –7.0 | –6.6 |

[a]The Drude model corresponds to the optimal choice of LJ parameters from the unscaled/vthole class of electrostatic models. The TIP3P[95] and SWM4-NDP[20] water models are used to accompany the CHARMM and Drude NMA models, respectively. Models are compared to QM calculations at the MP2/6-311+G(3df,2p) level, including a basis set superposition correction. The energies correspond to the minimum along the radial coordinate illustrated in Figure 2.

## TABLE 6

Summary of Drude Polarizable and Charmm NMA Properties[a]

| properties | experiment | CHARMM | Drude (unscaled/vthole) | Drude (scaled/vthole) |
|---|---|---|---|---|
| $\Delta H_{vap}$ ($T$ = 373 K), kcal/mol | –15.1, –13.8 | –13.4 ± 0.01 | –15.3 ± 0.01 | –14.2 ± 0.01 |
| $<v>$ ($T$ = 373 K), Å$^3$ | 135.9 | 133.0 ± 0.05 | 135.6 ± 0.05 | 134.6 ± 0.05 |
| $\Delta G_{hydr}$ ($T$ = 298 K), kcal/mol | –10.1 | –7.8 ± 0.2 | –10.9 ± 0.2 | –10.0 ± 0.2 |
| $\varepsilon$ ($T$ = 373 K) | 100.0 | 37 ± 2 | 92 ± 5 | 56 ± 2 |
| $\tau_D$ ($T$ = 308 K) | 590, 740 | 140 ± 20 | 660 ± 60 | 260 ± 40 |
| diffusion ($T$ = 373 K), Å$^2$/ps | 0.14, 0.12 | 0.20 ± 0.01 | 0.13 ± 0.01 | 0.17 ± 0.01 |

[a]The Drude model corresponds to the optimal choice of LJ parameters from the unscaled/vthole class of electrostatic models. The TIP3P[95] and SWM4-NDP[20] water models are used to solvate the CHARMM and Drude NMA models, respectively. Models are compared to experimental data.[10–13,77,78,98–101] The diffusion constant is calculated from a simulation at 373 K from the asymptotic time dependence of the mean-square displacement of the molecules as a function of time, $\langle \Delta r(t)^2 \rangle \rightarrow 6Dt$. The experimental diffusion constants correspond to a linear interpolation of available temperature-dependent data[101] to $T$ = 373K and an estimate at $T$ = 373K.[100] The MD results include a correction for finite size effects in periodic boundary conditions, $D = D_{pbc} + 2.837297 k_B T/(6\pi\eta L)$.[102] The viscosity at $T$ = 373 K is estimated from available temperature-dependent data, assuming $\eta \propto 1/T$.[101]

## TABLE 7

Summary of Drude Polarizable Neat Liquid Properties for Acetamide and *N*,*N*-Dimethylacetamide[a]

| properties | experiment | Drude (unscaled/vthole) | Drude (scaled/vthole) |
|---|---|---|---|
| | Acetamide | | |
| $\Delta H_{vap}$ ($T$ = 373 K), kcal/mol | –15.3, –14.6 | –15.0 ± 0.1 | –14.5 ± 0.1 |
| $<v>$ ($T$ = 373 K), kcal/mol | 100 | 103.0 ± 0.5 | 100.6 ± 0.5 |
| | *N*,*N*-Dimethyl Acetamide | | |
| $\Delta H_{vap}$ ($T$ = 298 K), kcal/mol | –10.9, –12.0, –16.2 | –14.8 ± 0.1 | –14.2 ± 0.1 |
| $<v>$ ($T$ = 298 K), kcal/mol | 154.5 | –153.2 ± 0.5 | 153.1 ± 0.5 |

[a]Models are compared to experimental data.[98,103]

## TABLE 8

Summary of Electrostatic Properties for the Amide Series[a,b]

| | \|μ\| (Debye) | | $\overline{TR(\alpha)}$ (Å$^3$) | | ⟨\|μ\|⟩ (Debye) | | | ε | |
|---|---|---|---|---|---|---|---|---|---|
| **molecule** | **QM** | **Drude** | **QM** | **Drude** | **CP** | **Drude** | **$G_K$, Drude** | **expt1** | **Drude** |
| acetamide | 4.0 | 4.0 | 5.9 | 6.1 | 6.0 | 5.8 | 2.4 ± 0.2 | 66.3 | 66 ± 3 |
| NMA | 3.9 | 3.9 | 7.8 | 7.9 | *5.9 | 5.7 | 4.6 ± 0.6 | 100 | 92 ± 5 |
| *N*,*N*-dimethyl acetamide | 4.0 | 3.9 | 9.6 | 9.5 | 5.2 | 5.0 | 1.7 ± 0.1 | 26 | 23 ± 1 |

[a]Properties of the Drude polarizable model are compared with QM and experimental data. The Drude model corresponds to the optimal choice of LJ parameters from the unscaled/vthole class of electrostatic models. Included is the gas-phase dipole (|μ|) and trace of the molecular polarizability ($\overline{\alpha}$). Also included is the average molecular dipole ⟨|μ|⟩ and Kirkwood $G_K$ factor calculated from neat liquid simulations at 373 K and the corresponding dielectric constant calculated from eq 7. The NMA CP simulation was run at $T$ = 308 K where ⟨|μ|⟩ = 6.0 Debye.[86] We estimate a drop in of ≈0.1 Debye for a simulation run at $T$ = 373 K on the basis of the behavior of the Drude polarizable model.